

Interpretation and theory of tunneling experiments on single nanostructures

Y. M. Niquet, C. Delerue,* and G. Allan

Institut d'Electronique et de Microélectronique du Nord, Département ISEN, Boîte Postale 69, F-59652 Villeneuve d'Ascq Cedex, France

M. Lannoo

Laboratoire Matériaux et Microélectronique de Provence, ISEM, Place Georges Pompidou, 83000 Toulon, France

(Received 22 October 2001; published 12 April 2002)

We discuss the interpretation of tunneling experiments on single molecules or semiconductor quantum dots weakly coupled to metallic electrodes. We identify the main features in the current-voltage curves and in the conductance using an extension of the theory of single charge tunneling. We analyze important quantities, such as the charging energy and the quasiparticle gap, providing simple rules to interpret the experiments. We discuss the limitations of the capacitance model to describe the system. We show that at a bias larger than the band-gap energy of the nanostructure the tunneling of both electrons and holes must be taken into account. We use self-consistent tight-binding calculations to illustrate these points and provide a comparison with recent experimental results on InAs nanocrystals.

DOI: 10.1103/PhysRevB.65.165334

PACS number(s): 73.63.Kv

I. INTRODUCTION

Recently remarkable experiments have been performed to measure the current I through single-quantum systems, such as molecules^{1–8} or semiconductor quantum dots.^{9–15} In these experiments, the molecules or the quantum dots are connected to metallic electrodes under bias V using scanning tunneling microscopy (STM) tips,^{1–4,9–13} nanometer-size electrodes^{5,14} or break junctions.^{6–8} Measurements show that the nanostructures do not behave like simple Ohmic resistors but display features arising from the quantum states of the system and from Coulombic effects, because a single excess charge on a molecule or a quantum dot dramatically influences its properties. Peaks in the conductance dI/dV characteristics are attributed to resonant tunneling through the molecular states or, in quantum dots, through the discrete levels induced by the confinement. In this perspective, quantum dots behave as artificial atoms whose properties can be tuned by varying their size.

Electrical studies give access to the intrinsic properties of nanostructures, provided that the coupling to the electrodes is weak. Thus one goal in the interpretation of tunneling experiments is to extract physically relevant quantities from the position of the peaks. For example, in the case of quantum dots, the scaling laws predicted for the variation with size of their band-gap and charging energies must be tested with accuracy. The possibility to deduce directly the energy gap of a nanostructure from the measurement of the current gap in the $I(V)$ curve and, more generally, the possibility to compare directly the experimental data with the results of theoretical calculations (e.g., single-particle spectra, quasiparticle spectra, etc.) is highly desirable. However the ability to extract this fundamental information from $I(V)$ or dI/dV characteristics is not straightforward. The presence of peaks in the dI/dV curves is due to the interplay between a discrete energy spectrum and charging effects. Another difficulty in the interpretation comes from the fact that electrical measurements not only probe transitions between different charge states of nanostructures, but also involve excited

states. For example, we have recently¹⁶ shown that, in the tunneling experiments of U. Banin *et al.*⁹ on InAs nanocrystals, peaks related to the injection of electron and holes are present in the same parts of the spectra. In that case the assignment of the peaks becomes more intricate.

Therefore, the aim of this paper is to investigate in detail difficulties common to the interpretation of the electrical measurements on single molecules or semiconductor quantum dots weakly coupled to metallic electrodes. Using an extension of the theory of Averin *et al.*¹⁷ for single charge tunneling, we identify the main features of $I(V)$ or dI/dV curves and we show how to connect them to quantities given by theoretical calculations. We provide simple rules that help to interpret the experiments. We analyze important quantities, such as the charging energy and the gap. We discuss the validity and the limitations of the capacitance model to describe the system as a double barrier junction. We establish the conditions for the injection of both electrons and holes into a nanostructure, and we discuss its effects on the spectroscopy. Finally we illustrate the discussion with the results of self-consistent tight-binding calculations on InAs nanocrystals¹⁶ that we compare with the experiments of Banin *et al.*⁹

II. GENERAL PROPERTIES OF THE $I(V)$ CURVES

A. Description of the system

We consider a system that can be described by a double barrier tunnel junction, as shown in Fig. 1. It consists of a semiconductor quantum dot or a molecule coupled to two metallic electrodes E1 and E2 by tunnel junctions $J1$ and $J2$. The electrodes E1 and E2 are characterized by their Fermi energies $\varepsilon_f^1 = \varepsilon_f - eV$ and $\varepsilon_f^2 = \varepsilon_f$. Electrons can tunnel through $J1$ and $J2$ with respective rates Γ^1 and Γ^2 which, in principle, depend on the energy of the tunneling electron. Due to its quantum size, the nanostructure is characterized by discrete energy levels. We assume¹⁸ that these levels are weakly coupled to the states in the electrodes so that, in this regime, the charge q of the nanostructure is well defined. At

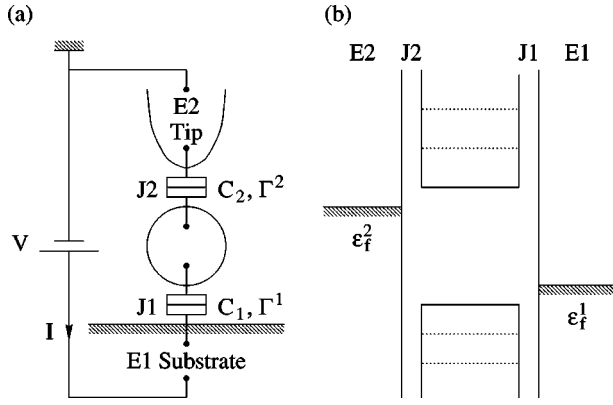


FIG. 1. Typical double barrier tunnel junction. (a) It consists of two metallic electrodes E1 and E2 (e.g., a substrate and the tip of a scanning tunneling microscope) weakly coupled to a nanostructure by two tunnel junctions $J1$ and $J2$ with capacitances C_1 and C_2 and tunneling rates Γ^1 and Γ^2 . (b) The metallic electrodes E1 and E2 are characterized by their Fermi energies $\varepsilon_f^1 = \varepsilon_f - eV$ and $\varepsilon_f^2 = \varepsilon_f$. The nanostructure is characterized by discrete energy levels.

a given q , the nanostructure can be in different electronic configurations (of index i) characterized by a total energy $E_i(q, V)$ (for simplicity, the charge q is defined in atomic units throughout the paper).

B. Transition levels

The main features of the $I(V)$ curve of such a system have already been discussed by several authors.^{17,19,20} The current I is the resultant of several tunneling processes. For example, an electron can tunnel from the electrode E1 to the nanostructure, which goes from a configuration of energy $E_i(q, V)$ to a configuration of energy $E_j(q-1, V)$. At $T \rightarrow 0$ K, this process is possible only if

$$\varepsilon_f^1 > \varepsilon_{ij}(q|q-1, V) = E_j(q-1, V) - E_i(q, V), \quad (1)$$

where we have defined transition levels with energy $\varepsilon_{ij}(q|q-1, V)$. The position of the transition levels with respect to the Fermi levels ε_f^1 and ε_f^2 determines which tunneling processes are possible at a given bias V . Therefore, at $T \rightarrow 0$ K, the $I(V)$ curve looks like a staircase, and the dI/dV curve consists of a series of peaks. The $I(V)$ curve exhibits a step each time a new channel is open for conduction through the system, i.e., when a Fermi level crosses a transition level. The amplitude of the step not only depends on the tunneling rates Γ^1 and Γ^2 , but also on the probabilities to find the nanostructure in the respective configurations^{17,19} (a calculation of these probabilities will be described in Sec. IV B). Thus the $I(V)$ curve has a direct interpretation in terms of the transition levels that, in principle, can be obtained theoretically by calculating the total energies $E_i(q, V)$. However, in practice, this procedure is either complex or most of the time impossible for the following reasons

(i) The transition levels depend on the bias V ; (ii) the number of charge states and electronic configurations to be considered may be important; (iii) the accurate calculation of the total energies using *ab initio* methods is only possible for

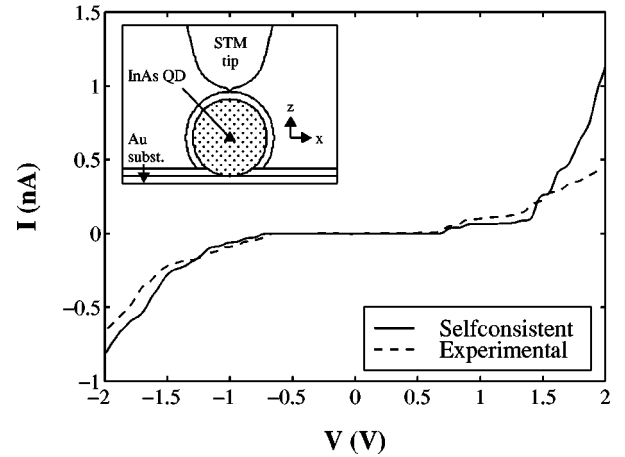


FIG. 2. Comparison between calculated (self-consistent) and experimental (Refs. 10,11) $I(V)$ curves for a 4.8-nm-diameter InAs nanocrystal. The self-consistent calculation was performed for the geometry shown in the inset and discussed in Sec. IV D.

small molecules or small semiconductor nanocrystals; and (iv) even if the coupling is weak, the total energy of the nanostructure strongly depends on the presence of the electrodes due to electrostatic interactions. Therefore, simplifications are usually necessary to allow a correct interpretation of the experiments. One goal of this paper is to discuss these approximations and their limitations.

C. A specific example: InAs nanocrystals on a gold substrate

We will illustrate the general discussion of this paper with a specific example corresponding to the experimental results of Banin and coworkers,⁹⁻¹¹ who reported tunneling spectroscopy experiments on InAs nanocrystals. The spherical InAs nanocrystals were prepared with colloidal techniques²¹ and linked to a gold substrate²² (electrode E1) with hexane dithiol molecules. The $I(V)$ curves were acquired on single InAs nanocrystals with a Pt-Ir STM tip (electrode E2) at $T = 4.2$ K. A typical $I(V)$ curve is shown in Fig. 2 for an InAs nanocrystal with diameter $d = 4.8$ nm.^{10,11} The corresponding conductance curve is plotted in Fig. 3. The two curves are typical of resonant tunneling processes through the discrete levels of the nanocrystal.

We have shown recently that a complete interpretation of these experiments is possible using a calculation of the tunneling current on the basis of self-consistent tight-binding framework.¹⁶ The electronic structure is obtained in tight binding with a Hamiltonian including the electrostatic potential, which is solution of the Poisson equation applied to a realistic geometry of the system. In this approximation, the screened electron-electron interactions are included at the Hartree level. The total energies are calculated, and the transition levels are obtained according to Eq. (1). Details on the geometry of the system and on the method are given in Ref. 16, and additional information is given in Appendixes A and B.

D. Evolution of the transition levels with the bias V

To simplify the interpretation of the electrical measurements on single nanostructures, a common approximation is

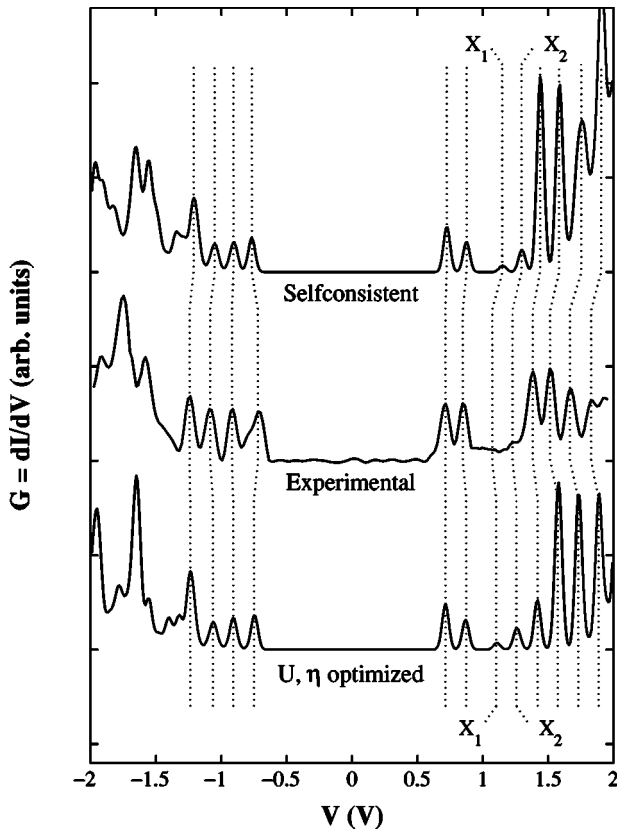


FIG. 3. Comparison between calculated and experimental differential conductance curves for a 4.8-nm-diameter InAs nanocrystal. The optimized parameters for the capacitive model are $U = 140$ meV and $\eta = 0.9$.

to assume that the transition energies have a linear dependence on the applied voltage V ,

$$\varepsilon_{ij}(q|q-1, V) = \varepsilon_{ij}(q|q-1) - \eta eV \quad (2)$$

with $0 \leq \eta \leq 1$. This is justified because the response of many systems to applied electric fields is linear. In the case of InAs nanocrystals, the self-consistent tight-binding calculations show that the linearity is verified within a few percents between -3 V and $+3$ V, in spite of the intense electric fields between the STM tip and the gold electrode. In the case of organic molecules, the linearity is also a good approximation within a broad range of voltages, as shown, for example, using self-consistent tight-binding calculations or using *ab initio* calculations in the local-density approximation (LDA).^{23,24}

In the general case, the slope η has a different value for each level $\varepsilon_{ij}(q|q-1)$. However, in the case of nanocrystals, we have found that the dispersion of the values is generally small, as shown in Fig. 4 where we plot η calculated for 50 levels both in the conduction and in valence bands of an InAs nanocrystal. In that case, a constant value of η for all the transition levels is a good approximation. To explain this result, we have plotted in Fig. 5 the corresponding electrostatic potential in the system for $V = 1$ V. Because the InAs nanocrystal has a higher dielectric constant than the surrounding medium (molecular layers, vacuum), the electric

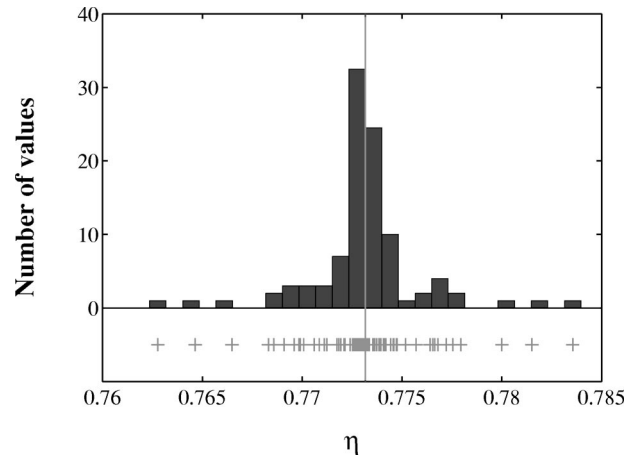


FIG. 4. Distribution of the values of η calculated for 50 levels both in the conduction and in valence bands of an InAs nanocrystal ($R = 3.2$ nm). The vertical line is the average value.

field is strongly screened in the semiconductor and the voltage drop between the two metallic electrodes mainly takes place in the regions with a low dielectric constant. Therefore, considering that the potential does not vary too much in the nanocrystal and that all the states are delocalized, the slope η cannot depend too much on the electronic configuration. The same effect occurs in molecular systems when the electronic states under consideration are all delocalized along the molecule.^{23–25} The π -conjugated oligomers, an important class of organic materials investigated for molecular electronics, usually belong to this category.²⁶ However, in the general case, where the molecular states are localized in different parts of the molecules, the values of η may be largely dispersed.²⁴ This effect may be used to build original molecular devices, such as molecular diodes, analogs of semiconductor p - n junctions²⁷ or of resonant tunneling diodes.

E. Addition and excitation spectra

In the following, we assume a constant slope $\eta > 0$. There are two situations where the interpretation of $I(V)$ spectra can be further simplified.²⁸ We describe them on a specific

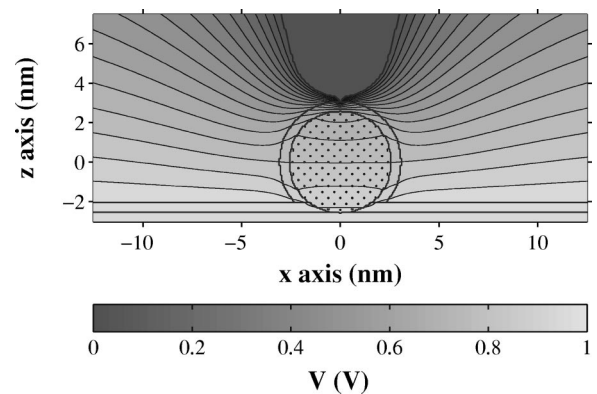


FIG. 5. Electrostatic potential inside an empty 4.8-nm-diameter InAs nanocrystal at bias $V = 1$ V.

example where, at positive bias, the electrons flow from the electrode E2 to the electrode E1 through the nanostructure. When $\Gamma^2 \gg \Gamma^1$, the nanostructure remains close to the equilibrium with the electrode E2. If the applied voltage increases, new channels open for the tunneling through J_2 . However, as the evacuation of the electrons through J_1 is not fast enough, the nanostructure remains charged with the maximum number of electrons, on average. Thus, the most visible steps in the $I(V)$ curve correspond to the opening of new charge states (addition steps, also called shell-filling spectroscopy²⁸). The experiments of Banin *et al.*⁹ are interpreted in this limit. In the opposite situation, where $\Gamma^2 \ll \Gamma^1$, the evacuation of the electrons is so fast that the nanocrystal cannot be charged by more than one electron, on average. Then, the most visible steps correspond to the transition levels associated to the excited configurations of one electron in the nanostructure (excitation steps, or shell-tunneling spectroscopy²⁸). We will show examples of $I(V)$ curves in such situations in Sec. IV C.

F. Coulomb charging

Here, we discuss the dependence of the transition levels with respect to the charge state of the nanostructure.

Most of the methods (Hartree, Hartree-Fock, LDA) used to calculate the electronic structure of quantum systems in different charge states lead to the resolution of a set of single-particle equations that must be solved self-consistently, the levels being filled by electrons according to the Pauli principle. A single-particle spectrum is obtained for each charge state q . The evolution of this spectrum with q is a consequence of electronic relaxation effects when charges are added to the system. In principle, the single-particle spectrum has no direct physical interpretation but, nevertheless, it is often at the heart of the interpretation of the experimental spectra.^{9–13,15} In that cases, the following approximations are made. (i) At a given q , the transition levels $\varepsilon_{ij}(q|q-1)$ are supposed to be directly related to the single-particle levels; and (ii) the addition of one electron to the system simply shifts the whole spectrum by a quantity U that describes the electronic repulsion in the system. In this approximation, the single-particle spectrum in the neutral charge state and the value of U are sufficient to define the whole set of transition levels. U is usually considered as a parameter. In the following, we discuss the validity of these approximations by comparing the situations of metallic islands and semiconductor quantum dots.

1. Metallic islands

Single charge tunneling in metallic islands has been extensively described in the literature.^{29,30} If the island is not too small, quantum confinement effects can be neglected and the transport is dominated by Coulomb blockade effects. The electrostatic energy of a charge q on the island is equal to $q^2/2(C_1+C_2)$ in terms of the junction capacitances C_1 and C_2 . Then the transition levels are simply given by

$$\varepsilon(q|q-1, V) = -qU + \Sigma - \eta eV \quad (3)$$

with $U = e^2/(C_1+C_2)$, $\Sigma = U/2$, and $\eta = C_1/(C_1+C_2)$. From this, it is clear that the linear variation of the transition levels with respect to V and to q is justified only in the case of metallic nanostructures where capacitances can be defined. In spite of this restriction, the capacitive model is often extended to the case of semiconductor quantum dots.^{17,19,20}

2. Semiconductor quantum dots

A common approximation^{17,19,20} is to write the total energy of a quantum dot charged with n electrons and p holes with respect to the neutral state as

$$E(\{n_i\}, \{p_i\}) = \sum_i n_i \varepsilon_i^e - \sum_i p_i \varepsilon_i^h + \eta eVq + \frac{1}{2}Uq^2, \quad (4)$$

where ε_i^e and ε_i^h are the electron and hole energy levels corresponding to the single-particle spectrum calculated in the neutral state. ε_1^h is often defined as the highest occupied ‘‘molecular’’ orbital (HOMO), and ε_1^e as the lowest unoccupied molecular orbital (LUMO). n_i and p_i are electron and hole occupation numbers, respectively; $n = \sum_i n_i$, $p = \sum_i p_i$, and $q = p - n$. By analogy with the metallic systems, the expression of U and Σ remains the same in terms of the capacitances (of course, they have not the same value as in the metallic case). In this single-particle picture, the tunneling of an electron between the electrodes and the energy level ε_i^e is determined by the position of the Fermi levels with respect to the transition level,

$$\varepsilon_i^e(q|q-1, V) = E(n_i=1, \{p_j\}) - E(n_i=0, \{p_j\}), \quad (5)$$

$$= \varepsilon_i^e - \eta eV - qU + \Sigma, \quad (6)$$

where Σ remains equal to $U/2$ in this approximation. In the same way, the tunneling of holes is defined by the transition levels

$$\varepsilon_i^h(q+1|q, V) = E(p_i=0, \{n_j\}) - E(p_i=1, \{n_j\}) \quad (7)$$

$$= \varepsilon_i^h - \eta eV - qU - \Sigma \quad (8)$$

The transition levels $\varepsilon_1^e(0|-1, V)$ and $\varepsilon_1^h(+1|0, V)$ correspond to the injection of an electron and a hole in the LUMO and the HOMO, respectively. At zero bias, they are simply given by

$$\varepsilon_1^e(0|-1) = \varepsilon_1^e + \Sigma, \quad (9)$$

$$\varepsilon_1^h(+1|0) = \varepsilon_1^h - \Sigma. \quad (10)$$

Their difference defines the quasiparticle gap E_g^{qp} of the quantum dot

$$E_g^{qp} = \varepsilon_1^e - \varepsilon_1^h + 2\Sigma, \quad (11)$$

which differs from the single-particle gap $E_g^0 = \varepsilon_1^e - \varepsilon_1^h$ by the quantity 2Σ , equal to U in the capacitive model. In the case of the experiments of Banin *et al.*⁹ on InAs nanocrystals, we have shown that this simple energetic model works well to describe quantitatively the observed spectra, the single-

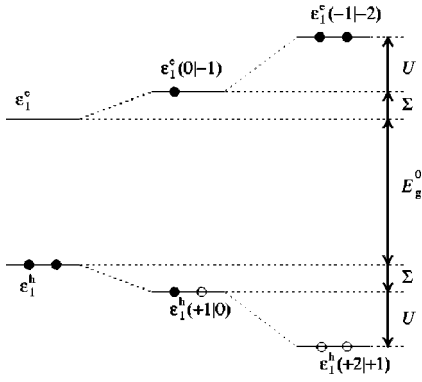


FIG. 6. Top: shift of the lowest conduction level due to the injection of one electron (Σ) or two electrons ($\Sigma + U$). Bottom: the situation for holes is symmetric.

particle levels being calculated in tight binding (Appendix A) and the capacitances being adjusted on the experiments.¹⁶ We analyze here the main reasons of this success by discussing first the case of isolated nanocrystals, and secondly the general case of a quantum dot embedded in a complex environment.

3. Isolated nanocrystals

Recent papers have shown that the quasiparticle spectrum of isolated molecules and small semiconductor nanocrystals (< 16 atoms) can be accurately predicted using *ab initio* GW calculations³¹ which goes beyond standard electronic structure calculations by including dynamical correlations between electrons.³² Recently, we have used an extension of the GW formalism in tight binding to calculate the quasiparticle gap of spherical silicon nanocrystals passivated by hydrogen atoms.³³ The situation that emerges from this work is summarized in Fig. 6. The lowest transition level (or quasiparticle level) for the injection of an electron in the quantum dot is shifted to higher energy with respect to ε_1^e by a quantity $\Sigma(R)$ that depends on the radius R of the nanocrystal. A good approximation³⁴ of $\Sigma(R)$ is given by the electrostatic self-energy of an electron in a dielectric sphere of radius R and of dielectric constant ϵ_{in} embedded in a material of dielectric constant ϵ_{out} ($=1$ in that case),

$$\Sigma(R) \approx \frac{1}{2} \left(\frac{1}{\epsilon_{out}} - \frac{1}{\epsilon_{in}} \right) \frac{e^2}{R} + \delta\Sigma(R), \quad (12)$$

where, when $\epsilon_{in} \gg \epsilon_{out}$, $\delta\Sigma(R)$ is given by

$$\delta\Sigma(R) \approx 0.47 \frac{e^2}{\epsilon_{in} R} \left(\frac{\epsilon_{in} - \epsilon_{out}}{\epsilon_{in} + \epsilon_{out}} \right). \quad (13)$$

These expressions represent the interaction energy of the electron with its own polarization charges at the surface of the dielectric sphere. Note that ϵ_{in} depends on R due to confinement effects.³⁴⁻³⁶ The calculated value of ϵ_{in} for InAs nanocrystals is given in Appendix A. GW calculations³³ justify the simple electrostatic description of the charging of a semiconductor quantum dot, as obtained in a more intuitive manner.^{37,34} The injection of a second electron leads to an

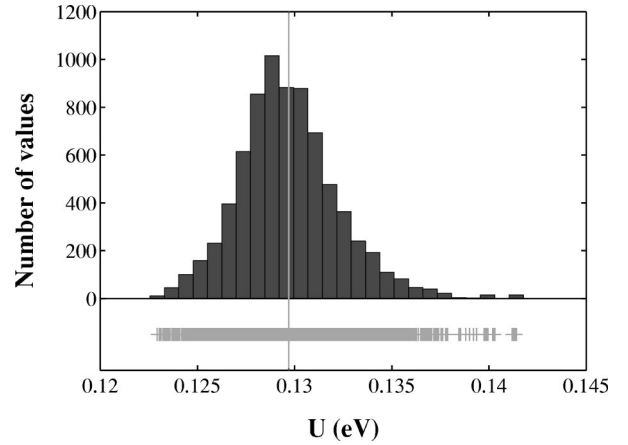


FIG. 7. Distribution of the values of the energies U_{ij}^{ee} , U_{ij}^{hh} , and U_{ij}^{eh} for 50 electron states and 50 hole states of an InAs nanocrystal ($R=3.2$ nm), in presence of metallic electrodes, with the geometry defined in the inset of Fig. 2. The vertical line is the average value.

additional upward shift $U(R)$ (Fig. 6) corresponding to the average Coulomb interaction between two electrons in the dielectric sphere. $U(R)$ not only includes the direct screened interaction, but also the interaction of one electron with the polarization charges induced by the second electron. With the same approximations as for $\Sigma(R)$, $U(R)$ is given well by^{37,34}

$$U(R) = \left(\frac{1}{\epsilon_{out}} + \frac{0.79}{\epsilon_{in}} \right) \frac{e^2}{R}. \quad (14)$$

The situation for holes is symmetric (Fig. 6). The highest quasiparticle levels are given by ε_1^h shifted similarly to lower energy.

4. General situation

The expressions of $\Sigma(R)$ and $U(R)$ have been obtained using a distribution of the electrons or the holes in the sphere given by an effective-mass wave function of the form $\sin(\pi r/R)/r$, which is only a good approximation for the HOMO and LUMO.³³ For the injection of carriers to the other states, the different forms of the wave functions must be considered, leading to different values of U . In addition, the medium surrounding the quantum dot is not homogeneous in the general case. Thus, the charging energy $Uq^2/2$ in Eq. (4) must be replaced by (see Appendix B)

$$\frac{1}{2} \sum_{i,j} n_i n_j U_{ij}^{ee} + \frac{1}{2} \sum_{i,j} p_i p_j U_{ij}^{hh} - \sum_{i,j} n_i p_j U_{ij}^{eh}. \quad (15)$$

In order to estimate the dispersion in energy which comes from this effect, we have calculated the values of U_{ij}^{ee} , U_{ij}^{hh} and U_{ij}^{eh} for 50 electron states and 50 hole states of an InAs nanocrystal in the presence of metallic electrodes. We see in Fig. 7 that the dispersion of U is actually small. The main reason is that the dominant contribution to U is the interaction between one carrier and the polarization charges induced by the other one, which does not depend too much on the details of the wave function. This is due to the fact that the

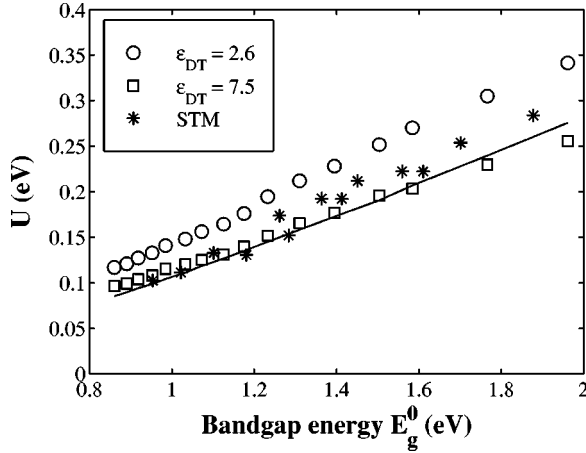


FIG. 8. Comparison between the calculated (tight-binding) and experimental (STM Ref. 9) charging energies U versus the bandgap energy E_g^0 for the geometry shown in the inset of Fig. 2. The dielectric constant of the hexane dithiol layer is either $\epsilon_{DT}=2.6$ or $\epsilon_{DT}=7.5$. Straight line: $U(R)$ given by Eq. (14) with $\epsilon_{out}=6$.

screening in the quantum dot is more efficient than in the surrounding medium (on average). This conclusion is in agreement with the experiments of Banin *et al.*,⁹ which show that the charging energy is approximately the same for the injection of an electron in a s or in a p state, or for the injection of a hole in the HOMO. The experimental values of U are plotted in Fig. 8 with respect to the radius R . Interestingly,^{38–40} these values are well fitted by $U(R)$ [Eq. (14)] with $\epsilon_{out}=6$ considered as an adjustable parameter. It may be surprising that it is possible to replace a complex medium made of vacuum, metallic electrodes and molecular layers around the nanocrystal by a homogeneous dielectric medium. We believe that this agreement simply reflects the $1/R$ dependence of the charging energy.

A numerical approach is usually required to calculate the charging energy in a general situation. However, the expression of $U(R)$ given in Eq. (14), established for an isolated nanocrystal, provides upper and lower bounds for the charging energy of a spherical dot surrounded by a complex dielectric medium. Because this medium cannot screen the electric fields more than a metal or less than vacuum, we can take the limits $\epsilon_{out} \rightarrow 1$ and $\epsilon_{out} \rightarrow \infty$,

$$\frac{0.79}{\epsilon_{in}} \frac{e^2}{R} < U < \left(1 + \frac{0.79}{\epsilon_{in}} \right) \frac{e^2}{R}. \quad (16)$$

The same argument can be applied to the self-energy Σ . These relations are useful to check the coherence of the interpretation of experimental data in terms of charging effects. The recent STM experiments on InAs (Ref. 9) and CdSe (Ref. 12) nanocrystals give charging energies that verify Eq. (16). In contrast, recent experiments¹⁴ on single-electron transistors based on CdSe nanocrystals give a charging energy of 14 ± 2 meV for a nanocrystal diameter of 5.5 nm, which is three times smaller than the lower bound of Eq. (16). One possible explanation of this discrepancy is that the

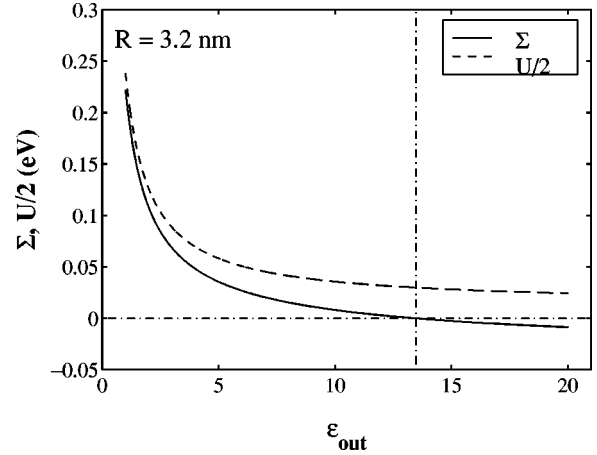


FIG. 9. Comparison between Σ and $U/2$ calculated as a function of ϵ_{out} in an InAs nanocrystal ($R=3.2$ nm). The vertical dashed line corresponds to $\epsilon_{out}=\epsilon_{in}=13.6$.

injected carriers are trapped on localized states, for example on surface defects where the charging energy can be considerably different.

When $\epsilon_{in} \rightarrow \infty$, one easily checks that $U(R) = 2\Sigma(R)$ corresponding to the case of a metallic island. Figure 9 shows that this relation remains a good approximation when $\epsilon_{in} \gg \epsilon_{out}$ because, once again, the dominant contribution in Σ and U comes from the interaction with the polarization charges at the surface. In consequence, when $\epsilon_{in} \gg \epsilon_{out}$, the capacitive model can be applied to semiconductor nanocrystals with a good degree of accuracy. The capacitances C_1 and C_2 can be adjusted in order to fulfill the relations $U \approx e^2/(C_1 + C_2)$, $\Sigma \approx U/2$, and $\eta \approx C_1/(C_1 + C_2)$, with U defined as an average value. The condition $\epsilon_{in} \gg \epsilon_{out}$ is easily realized experimentally, as the nanocrystal or the quantum dot is usually embedded in a material with a larger bandgap.

The conclusions of this section remain almost valid when the single-particle levels are calculated in LDA. However, a rigid shift must be applied to the conduction states with respect to the valence states to compensate the underestimation of the bulk semiconductor band gap in LDA. In the case of Si nanocrystals, this somehow empirical procedure is justified by *GW* calculations.³³

In all the examples considered in the previous discussion where confinement effects are large, single-particle approximations are justified, at least as a first step. However, in some cases, it may be necessary to consider exchange and correlation effects. For example, the experiments of Tarucha *et al.*^{41,15} on large GaAs quantum disks show that the charging energy is not a constant, depending, in particular, on the spin. Correlation effects between carriers injected into a quantum dot are usually treated using configuration interaction methods^{42,38,39} or in LDA.^{43,44}

III. INTERPRETATION OF THE CURRENT GAP

The current gap ΔV is the most striking feature of an $I(V)$ curve. It is defined by $\Delta V = V^+ - V^-$, where V^+ and V^- are the onsets of the current at positive and negative bias, respectively. It can be related to the quasiparticle gap E_g^{qp} of the

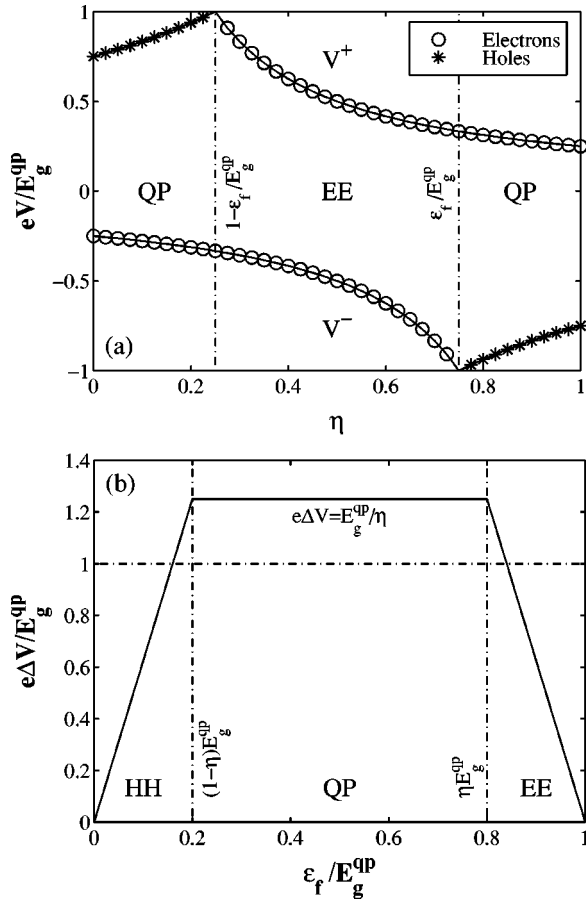


FIG. 10. (a) The onsets V^+ and V^- of the current at positive and negative bias as a function of η for fixed $\epsilon_f = 0.75E_g^{qp}$ ($\epsilon_1^h - \Sigma$ is taken as the zero energy, therefore $\epsilon_1^e + \Sigma = E_g^{qp}$). “Electrons” (“Holes”) mean that electrons (holes) first tunnel into the nanostructure. (b) The current gap ΔV as a function of ϵ_f for fixed $\eta = 0.8$. “QP” means that $\Delta V \sim E_g^{qp}$, “EE” (“HH”) means that electrons (holes) tunnel on both sides of the current gap.

nanostructure in certain conditions, which we discuss now.

We assume that the nanostructure is empty at zero bias, which means that the Fermi level ϵ_f is between $\epsilon_1^e(0|-1)$ and $\epsilon_1^h(+1|0)$. At positive bias, according to Eqs. (1) and (2), electrons can tunnel from the electrode E2 into the nanostructure when $eV > (\epsilon_1^e(0|-1) - \epsilon_f)/\eta$, and holes from the electrode E1 when $eV > -(\epsilon_1^h(+1|0) - \epsilon_f)/(1 - \eta)$. Therefore, the electrons first tunnel into the nanostructure if

$$\epsilon_f > \eta \epsilon_1^h(+1|0) + (1 - \eta) \epsilon_1^e(0|-1). \quad (17)$$

Similarly, at negative bias, the holes first tunnel into the nanostructure if

$$\epsilon_f < \eta \epsilon_1^e(0|-1) + (1 - \eta) \epsilon_1^h(+1|0). \quad (18)$$

The evolution of the current gap ΔV is shown in Fig. 10, as a function of η for fixed ϵ_f , or as a function of ϵ_f for fixed η . Three cases can be distinguished.

(i) Electrons tunnel on one side of the current gap, and holes tunnel on the other side: Then ΔV is proportional to the quasiparticle gap E_g^{qp} of the nanostructure.

$$e\Delta V = \frac{1}{\eta} E_g^{qp} \text{ if } \eta \geq \frac{1}{2}, \quad (19a)$$

$$e\Delta V = \frac{1}{1 - \eta} E_g^{qp} \text{ if } \eta \leq \frac{1}{2}. \quad (19b)$$

This regime is mainly obtained in asymmetrical systems where most of the applied voltage drops either across the junction $J1$ ($\eta \sim 0$) or $J2$ ($\eta \sim 1$). Moreover, the Fermi energy ϵ_f should be close to the midgap.

(ii) Electrons tunnel on both sides of the current gap:

$$e\Delta V = \frac{1}{\eta(1 - \eta)} (\epsilon_1^e(0|-1) - \epsilon_f), \quad (20)$$

where $e\Delta V$ can be much lower than the quasiparticle gap. This regime is likely to occur in symmetrical systems ($\eta \sim 1/2$) or when the Fermi energy ϵ_f is close to the electron levels of the nanostructure. η and ϵ_f can be calculated from the onsets V^+ and V^- ,

$$\eta = -V^-/\Delta V, \quad (21a)$$

$$\epsilon_f - \epsilon_1^e(0|-1) = eV^+V^-/\Delta V. \quad (21b)$$

(iii) Holes tunnel on both sides of the current gap:

$$e\Delta V = -\frac{1}{\eta(1 - \eta)} (\epsilon_1^h(+1|0) - \epsilon_f). \quad (22)$$

As in the former case, it is likely to occur in symmetrical systems or because ϵ_f is close to the hole levels of the nanostructure. Again, η and ϵ_f can be calculated from the onsets V^+ and V^- ,

$$\eta = V^+/\Delta V, \quad (23a)$$

$$\epsilon_f - \epsilon_1^h(+1|0) = -eV^+V^-/\Delta V. \quad (23b)$$

In the tunneling spectroscopy experiments based on a STM as in Ref. 9, E1 is a metallic substrate and E2 is the tip. η may easily be increased by retracting the tip from the nanocrystal. In most cases, $\eta > 1/2$ is achieved because the radius of curvature of the tip is much lower than that of the substrate. Cases (ii) and (iii) are usually distinguished from case (i) either because the current gap is much lower than the expected quasiparticle gap or because there are striking symmetries in the $I(V)$ staircase between positive and negative bias. Also note that in case (i) ΔV must decrease when retracting the tip (assuming $\eta \geq 1/2$). Case (ii) can be experimentally distinguished from case (iii) as follows. If electrons tunnel on both sides of the characteristics, $\eta = |V^-|/\Delta V$ should increase when retracting the tip (and thus $V^+/\Delta V$ decreases). On the contrary, if holes tunnel on both sides, then $\eta = V^+/\Delta V$ should increase when retracting the tip ($|V^-|/\Delta V$ decreases).⁴⁵

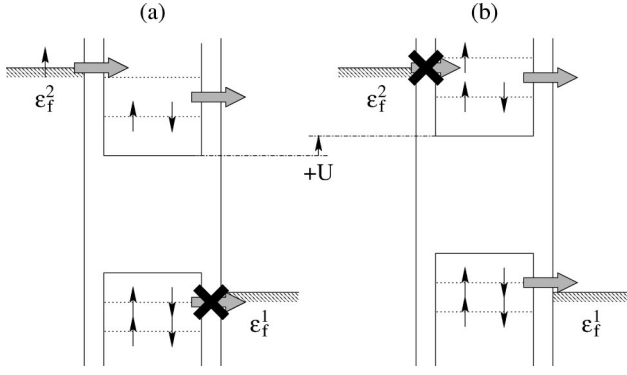


FIG. 11. Tunneling of both electrons and holes at large positive bias $eV > E_g^0$. (a) An electron tunnels from the electrode E2 into the nanostructure previously charged with $n_0 - 1$ electrons. The whole level structure is thus shifted to higher energy. (b) A first hole can now tunnel from the electrode E1 into the nanostructure charged with n_0 electrons.

IV. COMBINED ELECTRON-HOLE TRANSPORT

Just above V^+ or below V^- , usually only one type of carriers can tunnel into the nanostructure. However, when increasing further $|V|$, a new regime appears where both electrons and holes tunnel, complicating the interpretation of the $I(V)$ curve. We discuss here these situations.

A. Conditions for tunneling of both electrons and holes

We define by V_{eh}^+ (V_{eh}^-) the onset of this regime at positive (negative) bias. We focus on the case $\eta > 1/2$ and

$$\begin{aligned} \eta \epsilon_1^h(+1|0) + (1 - \eta) \epsilon_1^e(0|-1) < \epsilon_f \\ < \eta \epsilon_1^e(0|-1) + (1 - \eta) \epsilon_1^h(+1|0), \end{aligned} \quad (24)$$

where the current gap is proportional to the quasiparticle gap. Other cases are straightforward generalizations of this one. At positive bias just above V^+ , electrons tunnel from the electrode E2 into the nanostructure. The transition levels are shifted to higher energy each time an electron is added to the system [Fig. 11(a)]. For a sufficient number n_0 of electrons, the highest hole level crosses ϵ_f^1 and the injection of holes from the electrode E1 becomes possible [Fig. 11(b)]. Thus, two conditions must be verified;

$$\epsilon_f^2 \geq \epsilon_{n_0}^e(q+1|q, V), \quad (25)$$

$$\epsilon_f^1 \leq \epsilon_1^h(q+1|q, V). \quad (26)$$

Subtracting these two equations, one finds that the tunneling of holes in the system charged with n_0 electrons is possible only if

$$eV \geq \epsilon_{n_0}^e(q+1|q, V) - \epsilon_1^h(q+1|q, V) \approx \epsilon_{n_0}^e - \epsilon_1^h \geq E_g^0. \quad (27)$$

A similar relation can be derived at negative bias. Therefore, tunneling of either electrons or holes alone is ensured

only if $e|V|$ is smaller than E_g^0 , the single-particle gap (but eV_{eh}^+ may be much larger than E_g^0).

B. Theory of single charge tunneling including electron-hole transport

The interpretation of tunneling spectroscopy experiments usually relies on the so-called orthodox theory of single charge tunneling.^{29,30} In this section, we extend the theory of Averin *et al.*¹⁷ to include the transport of both electrons and holes. We assume that the relaxation rates in the system are fast enough with respect to the tunneling rates so that electrons and holes remain in equilibrium in their respective energy levels subsets $\{\epsilon_i^e\}$ and $\{\epsilon_i^h\}$. The recombination between electrons and holes will be introduced later in the master equations. Therefore, the single-particle distribution function $g_i^e(n)$ for n electrons in the nanostructure is¹⁷

$$g_i^e(n) = Z_e^{-1}(n) \sum_{\{n_j\}_n / n_i=1} \exp\left(-\beta \sum_j n_j \epsilon_j^e\right), \quad (28)$$

where

$$Z_e(n) = \sum_{\{n_j\}_n} \exp\left(-\beta \sum_j n_j \epsilon_j^e\right), \quad (29)$$

where $\{n_j\}_n$ stands for any configuration with n occupied energy levels ϵ_j^e and $\beta = 1/kT$. A similar expression holds for the single-particle distribution function $g_i^h(p)$ for p holes in the system. The total rates $\omega_{\pm}^{e\alpha}(n, p)$ for the tunneling of electrons through the junction $J\alpha$ into (+) or out of (-) the system charged with n electrons and p holes can be written¹⁷ as

$$\omega_+^{e\alpha}(n, p) = \sum_i \Gamma^\alpha f(\epsilon_i^e(q|q-1, V) - \epsilon_f^\alpha) [1 - g_i^e(n)], \quad (30a)$$

$$\omega_-^{e\alpha}(n, p) = \sum_i \Gamma^\alpha [1 - f(\epsilon_i^e(q+1|q, V) - \epsilon_f^\alpha)] g_i^e(n), \quad (30b)$$

where f is the Fermi-Dirac distribution function. The total rates $\omega_{\pm}^{h\alpha}(n, p)$ for the tunneling of holes can be written in the same way. The probability $\sigma_{n,p}$ to find n electrons and p holes is the solution of master equations

$$\begin{aligned} \frac{d}{dt} \sigma_{n,p} = & R(n+1, p+1) \sigma_{n+1, p+1} - R(n, p) \sigma_{n,p} \\ & + \omega_+^e(n-1, p) \sigma_{n-1, p} + \omega_-^e(n+1, p) \sigma_{n+1, p} \\ & + \omega_+^h(n, p-1) \sigma_{n, p-1} + \omega_-^h(n, p+1) \sigma_{n, p+1} \\ & - [\omega_+^e(n, p) + \omega_-^e(n, p) + \omega_+^h(n, p) + \omega_-^h(n, p)] \\ & \times \sigma_{n,p}, \end{aligned} \quad (31)$$

where

$$\omega_{\pm}^e(n, p) = \omega_{\pm}^{e1}(n, p) + \omega_{\pm}^{e2}(n, p), \quad (32a)$$

$$\omega_{\pm}^h(n,p) = \omega_{\pm}^{h1}(n,p) + \omega_{\pm}^{h2}(n,p). \quad (32b)$$

$R(n,p)$ is the recombination rate from the charge state (n,p) to the charge state $(n-1,p-1)$. In the case of a radiative recombination, we can write $R(n,p) = np/\tau$, where τ is the radiative lifetime. The current I through the structure is given by

$$I = I_1^e + I_1^h = I_2^e + I_2^h, \quad (33)$$

where

$$I_{\alpha}^e = (-1)^{\alpha} e \sum_{n,p} [\omega_{+}^{e\alpha}(n,p) - \omega_{-}^{e\alpha}(n,p)] \sigma_{n,p}, \quad (34a)$$

$$I_{\alpha}^h = -(-1)^{\alpha} e \sum_{n,p} [\omega_{+}^{h\alpha}(n,p) - \omega_{-}^{h\alpha}(n,p)] \sigma_{n,p}, \quad (34b)$$

where I_{α}^e and I_{α}^h are the electron and hole currents through the junctions $J\alpha$, respectively. The stationary solution of Eqs. (31) must be obtained under the constraint $\sum_{n,p} \sigma_{n,p} = 1$.

C. Calculation of the $I(V)$ curve in two limiting cases

In this section, we illustrate the effects of the tunneling of both electrons and holes on a simple model. We consider twofold degenerate single-particle energy levels ε_i^e and ε_i^h with a uniform distribution. We call δ_e and δ_h the splittings between successive levels. We assume constant tunneling rates Γ^1 and Γ^2 , a constant charging energy U , $\eta > 1/2$ and ε_f lying in the range of Eq. (24) such that electrons first tunnel when $V > 0$ and holes first tunnel when $V < 0$. We calculate the current in two limiting cases that do not depend on the recombination rate⁴⁶ $1/\tau$, namely, $\Gamma^2 \gg \Gamma^1$, and $\Gamma^1 \gg \Gamma^2$.

1. $\Gamma^2 \gg \Gamma^1$

In this case, the system remains close to equilibrium with the electrode E2. At $T \rightarrow 0$ K and at positive bias, the nanostructure is filled through $J2$ with the maximum possible number of electrons n_{max} (addition spectrum, see Sec. II E),

$$\sigma_{n,p} \sim \sigma_{n,p}^{eq} = \delta_{n,n_{max}} \delta_{p,0}. \quad (35)$$

Electrons slowly tunnel out of the nanostructure through $J1$ with a tunneling rate $n_{max}\Gamma^1$. When possible, holes also tunnel into the nanostructure through $J1$ with a tunneling rate $n_h\Gamma^1$, where n_h is the number of available hole channels (n_h is the number of hole transition levels above ε_f^1). These holes either rapidly tunnel out of the system through $J2$ or recombine with one electron. In summary, at positive bias

$$I = I_1^e + I_1^h = (n_{max} + n_h)e\Gamma^1. \quad (36)$$

Similar equations can be written at negative bias, the nanostructure being filled through $J2$ with the maximum possible number of holes p_{max} . A typical $I(V)$ curve in the case $\Gamma^2 \gg \Gamma^1$ is shown in Fig. 12. The onsets V_{eh}^+ and V_{eh}^- for

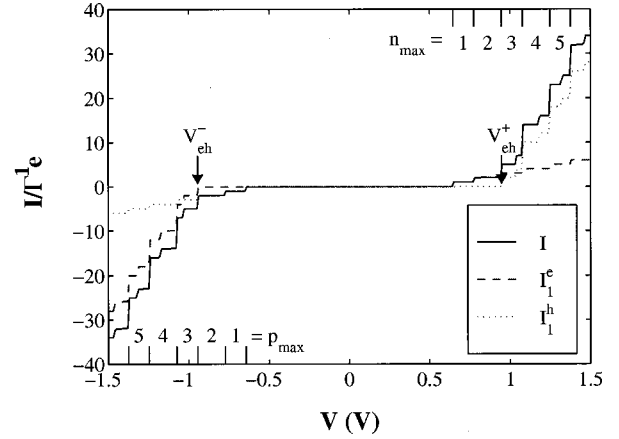


FIG. 12. Typical $I(V)$ curve in the case $\Gamma^2 \gg \Gamma^1$. The electron and hole currents I_1^e and I_1^h through the junction $J1$ are shown together with the total current I . The values of n_{max} , p_{max} , and the onsets for the tunneling of both electrons and holes V_{eh}^+ and V_{eh}^- are indicated. $U = 0.1$ eV, $\eta = 0.775$, $\varepsilon_1^h - \Sigma = 0$ eV, $\varepsilon_1^e + \Sigma = 1$ eV, $\delta_e = \delta_h = 33$ meV, and $\varepsilon_f = 0.5$ eV.

the injection of both electrons and holes at positive and negative bias correspond to $n_0 = 3$ and $p_0 = 3$, respectively. As long as $|V| < |V_{eh}^+|$, only addition steps are visible. In particular, an n -fold degenerate level gives rise to n successive addition steps. As soon as $V > V_{eh}^+$, holes tunnel into the nanostructure and the current increases rapidly with the number of available hole channels n_h . A few hole excitation steps may be present between two successive addition steps (one is actually visible between two successive addition steps in Fig. 12). However, addition steps usually remain the main features of the $I(V)$ staircase, since the addition of one electron into the system usually comes with the opening of new hole channels (actually four in Fig. 12).

2. $\Gamma^2 \ll \Gamma^1$

The system remains close to the equilibrium with the electrode E1. At positive bias, the nanostructure is filled through $J1$ with the maximum possible number of holes p_{max} . Thus, we have

$$I = I_2^e + I_2^h = (n_e + p_{max})e\Gamma^2, \quad (37)$$

where n_e is the number of available electron channels. Again, similar equations can be written at negative bias. A typical $I(V)$ curve is shown in Fig. 13. At positive bias, as long as $V < 1.33$ V, only electrons tunnel into the nanostructure through $J2$, but leave it through $J1$ before another electron is injected (excitation spectrum). The spacing between successive steps in the $I(V)$ staircase is thus directly proportional to the splitting between electron levels. Although tunneling of both electrons and holes is likely to occur as soon as $V > V_{eh}^+ = 0.9$ V ($n_0 = 1$), there is no hole injection until $V > 1.33$ V. Indeed, the probability $\sigma_{1,0}$ to find the electron needed for the tunneling of holes at $V = 0.9$ V is vanishing, because there is no charging of the system by the electrons. Holes sequentially fill the highest hole levels when V

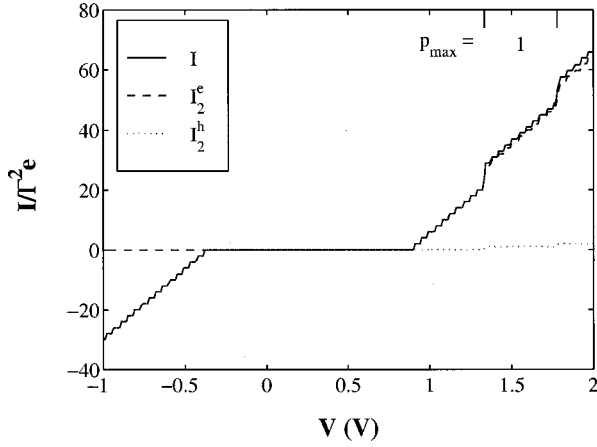


FIG. 13. Typical $I(V)$ curve for the case $\Gamma^1 \gg \Gamma^2$. The electron and hole currents I_2^e and I_2^h through junction $J2$ are shown together with the total current I . The value of p_{max} is indicated. Same parameters as in Fig. 12, except $\varepsilon_f = 0.3$ eV.

>1.33 V. Addition steps are then visible, even if they may be hardly separable from the closely spaced excitation steps.

We must note that both addition and excitation spectra may be seen on the same $I(V)$ curve whenever electrons or holes tunnel on both sides of the current gap in a highly asymmetric structure ($\Gamma^1 \gg \Gamma^2$ or $\Gamma^2 \gg \Gamma^1$). In that case, an addition spectrum will be seen on one side of the current gap and an excitation spectrum will be seen on the other side.

D. Experimental evidence of electron-hole transport

In this section, we discuss the interpretation of the tunneling spectroscopy experiments of Banin *et al.*^{9–11} on InAs nanocrystals. We consider, in particular, the $dI(V)/dV$ curve of Fig. 3. The tip was retracted from the nanocrystal so that η is close to 1. At positive bias, Banin *et al.* assigned the first group of two peaks to the tunneling of electrons filling the lowest, twofold degenerate $1S_e$ level with s -like symmetry, and the next group of four peaks to the tunneling of electrons filling the next, sixfold degenerate $1P_e$ level with p -like symmetry. At negative bias, they assigned the first group of four peaks and next group of three peaks to the tunneling of holes filling the highest fourfold degenerate $1H$ and $2H$ hole levels. This interpretation of the current gap and low-lying peaks is supported by the strong asymmetry of the $I(V)$ curve (Fig. 2) and by the fact that ΔV decreases when retracting the tip, which is a necessary condition for the quasiparticle gap to be measured if $\eta > 1/2$ (see Sec. III). However, we have shown¹⁶ that the tunneling of both electrons and holes at large voltages must be taken into account for a complete understanding of the tunneling spectrum. Here we give some further details and results.

The single-particle energy levels ε_i^e and ε_i^h of InAs nanocrystals are calculated with an orthogonal sp^3 tight-binding model described in Appendix A. We calculate the $I(V)$ curves with two different methods.

(i) We use the capacitive model of Eq. (4) with the energy levels calculated in tight binding for the isolated InAs nanocrystal and consider U , η as parameters.¹⁶ Although this

method gives reasonable results, one cannot realize whether the fitted U and η are consistent with the geometry of the problem.

(ii) We calculate the potential inside the nanocrystal with a finite differences method, starting from a realistic geometry (inset of Fig. 2). The nanocrystal is linked to the gold substrate by a 5-Å-thick hexane dithiol (DT) layer and is surrounded by a 5-Å-thick layer of molecular ligands (dielectric constant $\varepsilon_r = 2.6$). Another 5-Å-thick layer of molecular material is assumed adsorbed on the DT layer around the nanocrystal. The radius of curvature of the STM tip is $r = 2.5$ nm and the tip-nanocrystal distance is $d = 5$ Å. Concerning the DT layer, a dielectric constant $\varepsilon_{DT} = 2.6$ has been reported in the literature.⁴⁷ For reasons discussed below, we have considered either $\varepsilon_{DT} = 2.6$ or $\varepsilon_{DT} = 7.5$ in the calculations. We make a full self-consistent calculation¹⁶ of the single-particle states, the electrostatic potential, and the charging energies (see Appendix B). As shown in Fig. 8, the charging energy U calculated with this geometry is in good agreement with the experiments over the whole (2–8)-nm range.

With the method (i) we get $\eta \sim 0.9$ in most nanocrystals, meaning that most of the voltage drops across the tip-nanocrystal junction ($J2$). Such a high η is, however, difficult to obtain with a standard geometry (with comparable tip-nanocrystal distance and DT thickness) and with $\varepsilon_{DT} = 2.6$. In Ref. 16 we assumed that the nanocrystal was slightly flattened on the substrate side. Another way to achieve high η with a spherical nanocrystal is to decrease the thickness of the DT layer or to increase its dielectric constant up to 7.5. Indeed, the DT molecules may have been partly pushed out or there may be metallic contamination in the DT layer. All calculations presented here have been performed with a DT layer with a dielectric constant $\varepsilon_{DT} = 7.5$. The electrostatic potential $V_0(\vec{r})$ inside a neutral InAs nanocrystal at $V = 1$ V is shown in Fig. 5.

For a 4.8-nm-diameter InAs nanocrystal, we get $\varepsilon(1S_e) = 1.018$ eV, $\varepsilon(1P_e) = 1.368$ eV,⁴⁸ $\varepsilon(1H) = -0.158$ eV, and $\varepsilon(2H) = -0.186$ eV. The Fermi energy $\varepsilon_f = 0.445$ eV is obtained from the experimental position of the current gap.⁴⁹ Since an accurate calculation of the tunneling rates Γ^α is not possible, we take them as adjustable parameters. A detailed analysis of the relative height of the first steps⁵⁰ around the current gap suggests that $\Gamma^2 \approx 2\Gamma^1$. Thus we take $\Gamma^2 = 2\Gamma^1 = 6 \times 10^8$ s⁻¹ for the electrons and $\Gamma^2 = 2\Gamma^1 = 4 \times 10^8$ s⁻¹ for the holes. It is important to note that the position of the calculated conductance peaks does not depend on the tunneling rates Γ^α . Finally, we set $R(n, p) = np/\tau$ and $\tau = 1$ ns, which is characteristic of direct-gap semiconductors.

The self-consistent $I(V)$ curve calculated for a 4.8-nm-diameter InAs nanocrystal is shown in Fig. 2. The dI/dV curves, calculated with methods (i) and (ii) are shown in Fig. 3. The $I(V)$ and dI/dV curves were broadened with a Gaussian of width $\sigma = 25$ meV. The agreement with experiments is good, with practically a one to one correspondence between calculated and experimental peaks. Such a good agreement was also previously obtained for a 6.4-nm-diameter

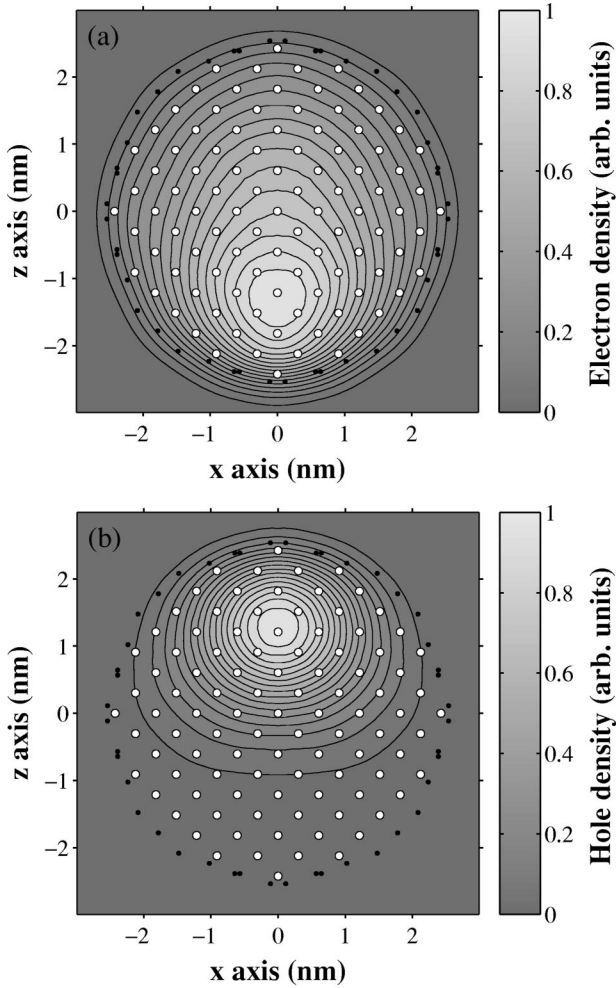


FIG. 14. Self-consistent (a) electron and (b) hole charge densities in a 4.8-nm-diameter nanocrystal charged with $n=3$ electrons and $p=1$ holes at bias voltage $V=1.5$ V. White dots are In/As atoms, black dots are H atoms.

InAs nanocrystal in Ref. 16. The optimized parameters for the capacitive model are $U=140$ meV and $\eta=0.9$ ($C_1=1.03$ aF and $C_2=0.11$ aF). We get $U\sim 140$ meV and $\eta\sim 0.82$ using non-self-consistent electron and hole charge densities calculated in the isolated nanocrystal. The self-consistency increases the effective η because the electrons and the holes localize in the tip-induced electric field, as shown in Fig. 14. With increasing V , the electrons localize near the gold substrate and the holes near the STM tip. The holes are more sensitive to the electric field because they have a higher effective mass than the electrons.

We now discuss the $I(V)$ and dI/dV curves in detail. At positive bias, the electrons first tunnel into the nanocrystal. The tunneling of holes only occurs when $V>V_{eh}^+$. We obtain $V_{eh}^+=1.57$ V ($n_0=4$) in the capacitive model and $V_{eh}^+=1.43$ V ($n_0=3$) in the self-consistent calculation, the difference being partly due to the sensitivity of the hole states to the tip-induced electric field. We confirm that the first group of two conductance peaks is assigned to the filling of the $1S_e$ level.⁹ There are also two excitation peaks X_1 and X_2 in Fig. 3 that are hardly visible on the experimental dI/dV curve.

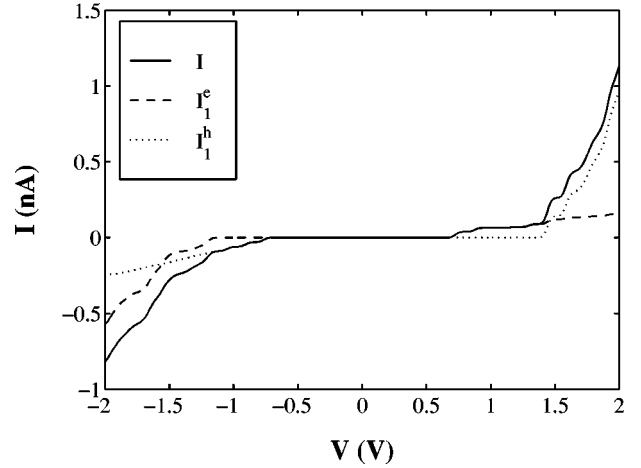


FIG. 15. $I(V)$ curve obtained with the self-consistent calculation showing the relative importance of the electron and hole currents I_1^e and I_1^h through the junction $J1$.

They are due to the tunneling of electrons onto the $1P_e$ level in the charge states $n=0$ and $n=1$. The next group of four peaks is mainly attributed to the tunneling of electrons filling the $1P_e$ level and to the tunneling of holes. The tunneling of holes is evidenced in Fig. 15 where we plot I_1^e and I_1^h . The hole current I_2^h through junction $J2$ is negligible—mainly electrons tunnel through junction $J2$ at positive bias. As discussed in Sec. IV C, addition peaks remain the main features of the $I(V)$ curve, and tunneling of holes mainly manifests as an increase in the current and as a broadening of the peaks due to the high density of hole states. The calculation overestimates the amplitude of the current at large positive bias (Fig. 2). Better agreement could be obtained in this range by dividing Γ^1 by 4 for the holes. This may arise because the hole states become strongly localized near the STM tip at large positive bias (Fig. 14).

The onset for electron tunneling at negative bias is $V_{eh}^- = -1.21$ V ($p_0=4$) in the capacitive model and $V_{eh}^- = -1.19$ V ($p_0=4$) in the self-consistent calculation. Due to the sensitivity of the hole states to the electric fields, the interpretation of the $I(V)$ curve in terms of the electronic structure of the isolated nanocrystal is quite hazardous at negative bias. Nevertheless, the first three peaks can be assigned to the tunneling of holes filling the highest hole level 1_H (although this level is split into two twofold degenerate levels by the electric field). The fourth peak involves the tunneling of holes and the tunneling of electrons onto the $1S_e$ electron level. Finally, the increase of the current below $V=-1.5$ V is mainly related to the tunneling of electrons onto the $1P_e$ electron level. This disagrees with the interpretation of Ref. 9 in terms of single hole transitions and makes difficult an experimental determination of the splittings between the hole states.¹⁶

V. CONCLUSION

We have extended the theory of single charge tunneling in a nanostructure including both single electron and hole charging effects. We have discussed the interpretation of tun-

TABLE I. Second nearest neighbor (NN) tight binding (TB) parameters for InAs and first NN TB parameters for pseudo-hydrogen atoms. The notation is that of Slater and Koster (Ref. 51) ($a = \text{As}$, $c = \text{In}$), In-H and As-H parameters being given in terms of two-center integrals. Neighbors positions are given in units of $a/4$ ($a = 6.053 \text{ \AA}$). Δ is the spin-orbit coupling. The numerical values are in eV.

Second NN TB parameters for InAs			
$E_{ss}^a(000)$	-6.61690	$E_{pp}^a(000)$	0.93191
$E_{ss}^c(000)$	-4.03536	$E_{pp}^c(000)$	3.17776
Δ^a	0.38100	Δ^c	0.27000
$E_{ss}(111)$	-1.51260		
$E_{sx}^{ac}(111)$	1.46298	$E_{sx}^{ca}(111)$	0.99029
$E_{xx}(111)$	0.24632	$E_{xy}(111)$	1.27524
$E_{ss}^a(220)$	-0.02037		
$E_{sx}^a(220)$	-0.28406	$E_{sx}^a(022)$	0.01623
$E_{xx}^a(220)$	-0.03888	$E_{xx}^a(022)$	-0.13087
$E_{xy}^a(220)$	-0.08055	$E_{xy}^a(022)$	-0.17846
$E_{ss}^c(220)$	-0.04965		
$E_{sx}^c(220)$	0.22357	$E_{sx}^c(022)$	-0.05660
$E_{xx}^c(220)$	0.36088	$E_{xx}^c(022)$	-0.45711
$E_{xy}^c(220)$	0.14806	$E_{xy}^c(022)$	0.02651
1 st NN TB parameters for In-H and As-H			
E_H	0.00000		
$V_{ss\sigma}$	-3.50000	$V_{sp\sigma}$	4.50000

neling experiments, and we have shown how to connect the features in the current-voltage curves to quantities given by theoretical calculations. Using a self-consistent tight-binding approach, we have revisited the interpretation of recent tunneling spectroscopy experiments on InAs nanocrystals, showing that tunneling of both electrons and holes profoundly affects the current-voltage curve. Our work shows that a quantitative simulation of transport properties in nanostructures is nowadays possible starting from electronic structure calculations.

ACKNOWLEDGMENTS

The Institut d'Electronique et de Microélectronique du Nord is UMR 8520 of CNRS and the Laboratoire Matériaux et Microélectronique de Provence is UMR 6137 of CNRS. We thank O. Millo for fruitful discussions.

APPENDIX A: TIGHT-BINDING CALCULATIONS ON InAs NANOCRYSTALS

The single-particle energy levels ε_i^e and ε_i^h of InAs nanocrystals are calculated with an orthogonal sp^3 tight-binding model including up to second nearest-neighbor interactions. The tight-binding parameters (Table I) are fitted to the bulk InAs band structure calculated in LDA corrected for the band-gap problem, and to the experimental effective masses⁵² (Table II). Spin-orbit coupling is included. The surface dangling bonds are saturated with pseudohydrogen atoms. The calculated band gap E_g^0 of InAs nanocrystals given

TABLE II. Comparison between experimental (Ref. 53) (Exp) and tight binding (TB) bulk band-gap energy, conduction band (CB) effective masses and valence band (VB) Luttinger parameters for InAs. m_0 is the free electron mass.

	Exp	TB
Direct band-gap energy		
E_g^{bulk}	0.418	0.406 eV
CB effective mass		
m^*	$0.023m_0$	$0.023m_0$
VB Luttinger parameters		
γ_1	19.70	19.50
γ_2	8.40	8.42
γ_3	9.28	9.20

in Ref. 16 is in good agreement with tunneling spectroscopy data. The splittings between the $1S_e$ and $1P_e$ electron levels and between the $1H$ and $2H$ hole levels have also been discussed in Ref. 16. The confinement energy of the $1H$, $1S_e$, and $1P_e$ levels are fitted over the (2–8)-nm range with the following expression:⁵²

$$\varepsilon = \frac{K}{d^2 + ad + b}. \quad (\text{A1})$$

d is the diameter of the nanocrystal in nanometers. The top of the bulk InAs valence band is taken as the zero energy. The parameters K , a , and b are given in Table III.

The macroscopic dielectric constant of the nanocrystal $\varepsilon_{in}(d) = \varepsilon_{in}^\infty(d) + \Delta \varepsilon_{in}^{ion}$ includes an electronic contribution $\varepsilon_{in}^\infty(d)$ and a ionic correction $\Delta \varepsilon_{in}^{ion}$ that we assume to be size independent. The electronic contribution is calculated for small nanocrystals in tight binding as in Ref. 34 and is extrapolated to large diameters d with a Penn model.⁵⁴ Thus we obtain

$$\varepsilon_{in}^\infty(d) = 1 + (\varepsilon_{bulk}^\infty - 1) \left(\frac{E_g^{bulk} + \Delta}{E_g^0(d) + \Delta} \right)^2, \quad (\text{A2})$$

where $\varepsilon_{bulk}^\infty = 11.08$, $E_g^{bulk} = 0.406 \text{ eV}$, and $\Delta = 5.644 \text{ eV}$. We set $\Delta \varepsilon_{in}^{ion} = 4.07$ to get the correct bulk dielectric constant⁵³ $\varepsilon_{in}^{bulk} = 15.15$.

TABLE III. Fits to the energy of the $1H$, $1S_e$, and $1P_e$ levels using the expression $a = K/(d^2 + ad + b)$. d is the diameter of the InAs nanocrystal in nanometers. The top of the bulk InAs valence band is taken as the zero energy.

	$K(\text{eV nm}^{-2})$	$a(\text{nm})$	$b(\text{nm}^2)$
$\varepsilon(1H)$	7.966	5.189	0.066
$\varepsilon(1S_e)$	92.800	22.649	20.508
$\varepsilon(1P_e)$	158.622	21.676	37.244

APPENDIX B: SELF-CONSISTENT CALCULATION OF THE $I(V)$ CURVES

In this appendix, we detail the self-consistent calculation of the $I(V)$ curves. The electrostatic potential inside the nanocrystal is calculated with a standard finite differences method. A cylindrical symmetry is assumed. The total energy of the nanocrystal is written as

$$E(\{n_i\}, \{p_i\}, V) = \sum_i n_i (\varepsilon_i^e - \eta_i^e eV) - \sum_i p_i (\varepsilon_i^h - \eta_i^h eV) + U(n, p), \quad (\text{B1})$$

where, for $\alpha = e, h$,

$$\eta_i^\alpha = \langle \Psi_i^\alpha | V_0(\vec{r}) | \Psi_i^\alpha \rangle / V_{ref}. \quad (\text{B2})$$

Ψ_i^e and Ψ_i^h are the wave functions of energy ε_i^e and ε_i^h and $V_0(\vec{r})$ is the electrostatic potential in the neutral nanocrystal at $V = V_{ref}$.⁵⁵ The charging energy $U(n, p)$ is calculated in the Hartree approximation,

$$U(n, p) = \frac{1}{2} \sum_{\substack{i \leq n \\ j \leq n}} U_{ij}^{ee} + \frac{1}{2} \sum_{\substack{i \leq p \\ j \leq p}} U_{ij}^{hh} - \sum_{\substack{i \leq n \\ j \leq p}} U_{ij}^{eh}, \quad (\text{B3})$$

where, for $\alpha = e, h$ and $\beta = e, h$,

$$U_{ij}^{\alpha\beta} = \int |\Psi_i^\alpha(\vec{r})|^2 V_j^\beta(\vec{r}) d^3\vec{r}. \quad (\text{B4})$$

$V_j^\beta(\vec{r})$ is the electrostatic potential created by the cylindrically averaged density $|\Psi_j^\beta|^2(\vec{r})$ at zero bias. In principle,

$U_{ii}^{ee}/2$ and $U_{ii}^{hh}/2$ should be replaced by the self-energies Σ_i^e and Σ_i^h . However, the calculation is not possible in the cylindrical symmetry. Therefore, we simply remove from U_{ii}^{ee} and U_{ii}^{hh} the self-interaction term included in the Hartree energy. For that purpose, we define approximate self-energies Σ_i^α ($\alpha = e, h$),

$$2\Sigma_i^\alpha = U_{ii}^\alpha - \int \int |\Psi_i^\alpha(\vec{r})|^2 \frac{e^2}{\varepsilon_{in} |\vec{r} - \vec{r}'|} |\Psi_i^\alpha(\vec{r}')|^2 d^3\vec{r} d^3\vec{r}'. \quad (\text{B5})$$

This procedure slightly underestimates the self-energy in spherical nanocrystals embedded in a homogenous medium with dielectric constant $\varepsilon_{out} < \varepsilon_{in}$.

The ground-state energy is self-consistently computed for a set of charge states (n, p) and several bias voltages V_i . The self-interaction correction [Eq. (B5)] is made *a posteriori*. The self-consistent wave functions Ψ_i^e and Ψ_i^h are developed in the subspace spanned by the lowest N_H hole states and N_E electron states of the isolated nanocrystal ($N_H = 240$ and $N_E = 120$). The self-consistency is rapidly achieved with the ‘‘optimal damping algorithm’’ mixing scheme.⁵⁶ The ground-state energy is interpolated in the whole range of V with a third order polynomial. The energies of the excited configurations are approximated by the single-particle spectrum of the corresponding ground state. The calculation of the $I(V)$ curve is performed at $T = 0$ K so that the nanocrystal is in its ground state before each tunneling process.

*Electronic address: Christophe.Delerue@isen.fr

¹R.P. Andres, J.D. Bielefeld, J.I. Henderson, D. B. Janes, V. R. Kolagunta, C.P. Kubiak, W.J. Wahoney, and R.G. Osifchin, *Science* **273**, 1690 (1996).

²L.A. Bumm, J.J. Arnold, M.T. Cygan, T.D. Dunbar, T.P. Burgin, L. JonesII, D.L. Allara, J.M. Tour, and P.M. Weiss, *Science* **271**, 1705 (1996).

³A. Stabel, P. Herwig, K. Müllen, and J.P. Rabe, *Angew. Chem. Int. Ed. Engl.* **34**, 1609 (1995).

⁴W. Tian, S. Datta, S. Hong, R. Reifenberger, J.I. Henderson, and P. Kubiak, *J. Chem. Phys.* **109**, 2874 (1998).

⁵J. Tans, M.H. Devoret, H. Dai, A. Hess, R.E. Smalley, L. Geerligs, and C. Dekker, *Nature (London)* **386**, 474 (1997).

⁶M.A. Reed, C. Zhou, C.J. Muller, T.P. Burgin, and J.M. Tour, *Science* **278**, 252 (1997).

⁷J. Chen, M.A. Reed, A.M. Rawlett, and J. M. Tour, *Science* **286**, 1550 (1999).

⁸C. Kergueris, J.-P. Bourgoin, S. Pasacín, D. Esteve, C. Urbina, M. Magoga, and C. Joachim, *Phys. Rev. B* **59**, 12 505 (1999).

⁹U. Banin, Y.W. Cao, D. Katz, and O. Millo, *Nature (London)* **400**, 542 (1999).

¹⁰O. Millo, D. Katz, Y. Levi, Y.W. Cao, and U. Banin, *J. Low Temp. Phys.* **118**, 365 (2000).

¹¹O. Millo, D. Katz, Y.W. Cao, and U. Banin, *Phys. Rev. B* **61**, 16 773 (2000).

¹²B. Alpers, I. Rubinstein, G. Hodes, D. Porath, and O. Millo, *Appl. Phys. Lett.* **75**, 1751 (1999).

¹³E.P.A.M. Bakkers and D. Vanmaekelbergh, *Phys. Rev. B* **62**, R7743 (2000).

¹⁴D.L. Klein, R. Roth, A.K.L. Lim, A.P. Alivisatos, and P.L. McEuen, *Nature (London)* **389**, 699 (1997).

¹⁵L.P. Kouwenhoven, D.G. Austing, and S. Tarucha, *Rep. Prog. Phys.* **64**, 701 (2001).

¹⁶Y.M. Niquet, C. Delerue, G. Allan, and M. Lannoo, *Phys. Rev. B* **64**, 113305 (2001).

¹⁷D.V. Averin, A.N. Korotkov, and K.K. Likharev, *Phys. Rev. B* **44**, 6199 (1991).

¹⁸The theory does not apply to the important class of systems where molecules are chemically grafted to the electrodes.

¹⁹C.W.J. Beenakker, *Phys. Rev. B* **44**, 1646 (1991).

²⁰R.I. Shekhter, *Zh. Éksp. Teor. Fiz.* **63**, 1410 (1972) [*Sov. Phys. JETP* **36**, 747 (1973)]; I.O. Kulik and R.I. Shekhter, *ibid.* **68**, 623 (1975) [*ibid.* **41**, 308 (1975)].

²¹A.A. Guzelian, U. Banin, A.V. Kadavanich, X. Peng, and A.P. Alivisatos, *Appl. Phys. Lett.* **69**, 1432 (1996).

²²V.L. Colvin, A.N. Goldstein, and A.P. Alivisatos, *J. Am. Chem. Soc.* **114**, 5221 (1992).

²³C. Krzeminski, C. Delerue, G. Allan, D. Vuillaume, and R.M. Metzger, *Phys. Rev. B* **64**, 085405 (2001).

²⁴C. Krzeminski, C. Delerue, and G. Allan, *J. Phys. Chem. B* **105**, 6321 (2001).

- ²⁵S. Datta, W. Tian, S. Hong, R. Reifengerger, J.I. Henderson, and C.P. Kubiak, *Phys. Rev. Lett.* **79**, 2530 (1997).
- ²⁶C. Krzeminski, C. Delerue, G. Allan, V. Haguët, D. Stiévenard, P. Frère, E. Levillain, and J. Roncali, *J. Chem. Phys.* **111**, 6643 (1999).
- ²⁷A. Aviram and M. Ratner, *Chem. Phys. Lett.* **29**, 277 (1974).
- ²⁸D. Vanmaekelbergh, E.P.A.M. Bakkers, A. Franceschetti, A. Zunger, L. Gurevich, L. Canali, M. Janus, and L.P. Kouwenhoven, *Nano Letters* **1**, 551 (2001).
- ²⁹*Single Charge Tunneling: Coulomb Blockade Phenomena in Nanostructures*, edited by H. Grabert and M.H. Devoret (Plenum Press, New York, 1992).
- ³⁰D.K. Ferry and S.M. Goodnick, *Transport in Nanostructures* (Cambridge University Press, Cambridge, England, 1997).
- ³¹L. Hedin and S. Lundqvist, *Solid State Phys.* **23**, 1 (1969).
- ³²G. Onida, L. Reining, R.W. Godby, R. DelSole, and W. Andreoni, *Phys. Rev. Lett.* **75**, 818 (1995); M. Rohlfing and S.G. Louie, *ibid.* **80**, 3320 (1998).
- ³³C. Delerue, M. Lannoo, and G. Allan, *Phys. Rev. Lett.* **84**, 2457 (2000).
- ³⁴M. Lannoo, C. Delerue, and G. Allan, *Phys. Rev. Lett.* **74**, 3415 (1995).
- ³⁵L.W. Wang and A. Zunger, *Phys. Rev. Lett.* **73**, 1039 (1994).
- ³⁶R. Tsu and D. Babic, *Appl. Phys. Lett.* **64**, 1806 (1994).
- ³⁷L.E. Brus, *J. Chem. Phys.* **79**, 5566 (1983); **80**, 4403 (1984).
- ³⁸A. Franceschetti and A. Zunger, *Phys. Rev. B* **62**, 2614 (2000).
- ³⁹M. Rontani, F. Rossi, F. Manghi, and E. Molinari, *Phys. Rev. B* **59**, 10 165 (1999).
- ⁴⁰A. Franceschetti, A. Williamson, and A. Zunger, *J. Phys. Chem.* **104**, 3398 (2000).
- ⁴¹S. Tarucha, D.G. Austing, T. Honda, R.J. Van der Hage, and L.P. Kouwenhoven, *Phys. Rev. Lett.* **77**, 3613 (1996).
- ⁴²E. Martin, C. Delerue, G. Allan, and M. Lannoo, *Phys. Rev. B* **50**, 18 258 (1994).
- ⁴³K. Hirose and N.S. Wingreen, *Phys. Rev. B* **59**, 4604 (1999).
- ⁴⁴S. Nagaraja, P. Matagne, V.-Y. Thean, J.-P. Leburton, Y.-H. Kim, and R.-M. Martin, *Phys. Rev. B* **56**, 15 752 (1997).
- ⁴⁵One must take care that ε_f may also vary when retracting the tip.
- ⁴⁶With constant tunneling rates Γ^1 and Γ^2 , τ only affects the relative contribution of electron and hole currents through junctions J_1 and J_2 , but has no influence on the total current I .
- ⁴⁷M.D. Porter, T.B. Bright, D.L. Allara, and C.E.D. Chidsey, *J. Am. Chem. Soc.* **109**, 3559 (1987).
- ⁴⁸The spin-orbit coupling splits the sixfold degenerate p -like state into one twofold and one fourfold degenerate state.
- ⁴⁹We have taken into account a 0.5 V built-in potential in the self-consistent calculation (work function difference between E1 and E2). However, this built-in potential has minor influence on the $I(V)$ curves.
- ⁵⁰The relative amplitude of the two current steps I_1 and I_2 associated with the twofold degenerate $1S_e$ levels is $I_2/I_1 = (1 + 2\alpha)/(1 + \alpha)$, where $\alpha = \Gamma_2/\Gamma_1$.
- ⁵¹J.C. Slater and G.F. Koster, *Phys. Rev.* **94**, 1498 (1954).
- ⁵²Y.M. Niquet, C. Delerue, G. Allan, and M. Lannoo, *Phys. Rev. B* **62**, 5109 (2000).
- ⁵³O. Madelung, in *Numerical Data and Functional Relationship in Science and Technology, Physics of Group IV Elements and III-V Compounds*, Landolt-Börnstein, New Series, Group III, Vol. 17, pt. a (Springer-Verlag, Berlin, 1992).
- ⁵⁴D.R. Penn, *Phys. Rev.* **128**, 2093 (1962).
- ⁵⁵The degenerate wave functions of the nanocrystal are first sorted according to the irreducible representations of the C_{2v} group.
- ⁵⁶E. Cancès and C. Le Bris, *Int. J. Quantum Chem.* **79**, 82 (2000).